

Significant improvement in the accuracy of simulated chaotic N -body orbits by using smoothness

David M. Hernandez^{1,2} 

¹Harvard–Smithsonian Center for Astrophysics, 60 Garden St., MS 51, Cambridge, MA 02138, USA

²RIKEN Advanced Institute for Computational Science, 7-1-26 Minatojima-minami-machi, Chuo-ku, Kobe, 650-0047 Hyogo, Japan

9 April 2019

ABSTRACT

Symplectic integrators are a foundation to the study of dynamical N -body phenomena, at scales ranging from planetary to cosmological. These integrators preserve the Poincaré invariants of Hamiltonian dynamics. The N -body Hamiltonian has another, perhaps overlooked, symmetry: it is perfectly smooth for particle separations greater than 0. Many popular symplectic integrators, such as hybrid methods or block adaptive stepping methods, do not respect this symmetry and it is perhaps unclear whether they should. We investigate the importance of this symmetry by considering hybrid integrators, whose smoothness can be tuned easily. Hybrid methods are perfectly smooth, except at a finite number of phase space points. We study chaotic planetary orbits in a test considered by [Wisdom](#). We find that increasing smoothness, at negligible extra computational cost in particular tests, improves the Jacobi constant error of the orbits by about 5 orders of magnitude in long-term simulations. The results from this work suggest that smoothness of the N -body problem is a symmetry worth preserving in simulations.

Key words: methods: numerical—celestial mechanics—globular clusters: general—galaxies:evolution—Galaxy: kinematics and dynamics—planets and satellites: dynamical evolution and stability

1 INTRODUCTION

Symplectic integrators have been successful at studying a wide range of N -body particle dynamics in astrophysics and beyond, from planetary systems to galaxies with dark matter. They are usually severely limited in that they require a timestep, but gravitation has no timescales associated with it. To combat this limitation, a number of techniques have been employed ([Hernandez 2019](#)) such as block timestepping or hybrid integration, which have become the basis of popular dynamics codes. These modifications change the smoothness of the N -body integrator. The N -body Hamiltonian is a C^∞ function for the domain of separations greater than 0, meaning it can get differentiated infinite times with respect to phase space coordinates and still be defined. Traditional symplectic integrators constructed through operator splitting ([Yoshida 1990](#); [Wisdom & Holman 1991](#)) respect this symmetry of the N -body Hamiltonian and are still C^∞ . However, hybrid integrators ([Chambers 1999](#); [Rein et al. 2019](#); [Hernandez 2019](#); [Wisdom 2017](#)) are C^n , where n is an integer satisfying $n \geq 0$. A C^n function can be differentiated n times and still be continuous. Block time-stepping methods [Farr & Bertschinger \(2007\)](#) and integrator subcycling methods [Springel \(2005\)](#); [Duncan et al. \(1998\)](#) are not

derived from smooth Hamiltonians; they switch in analogy to the ‘modified Heaviside function’ from [Rein et al. \(2019\)](#). It remains to be seen whether Hamiltonian smoothness is a symmetry which integrators, whether they are symplectic or not, should mimic, just as they might mimic the conservation of Poincaré invariants, the existence of a global Hamiltonian ([Hairer et al. 2006](#), Section IX.3.2), the time-reversibility ([Hernandez & Bertschinger 2018](#)), or the angular and total momentum conservation.

[Hernandez \(2019\)](#) has explored the question of integrator smoothness for regular orbits. The work considered hybrid integrators, because it is simple to modify their smoothness by changing the functional form of the transition function. Hybrid integrators are C^∞ except at a finite number of position coordinates. Consistent with the predictions of [Arnaud & Xue \(2016\)](#), [Hernandez \(2019\)](#) found that only smoothness of at least $C^{1.1}$ yielded periodic orbits. The results were verified using a 1D and 2D Kepler problem Hamiltonian and a simple harmonic oscillator Hamiltonian. Increasing the smoothness past $C^{1.1}$ did not provide additional benefit as the long-term errors already oscillated. Data from Figure 8 in [Hernandez \(2019\)](#) show that integrations using the C^∞ transition function had smaller error amplitudes than the integrations with the $C^{1.1}$ function. The importance of the precise size of these amplitudes is questionable ([Portegies Zwart & Boekholt 2014](#); [Boekholt & Portegies Zwart 2015](#)), and simple techniques

* Email: dmhernandez@cfa.harvard.edu, david.hernandez@riken.jp

already exist to reduce them (Wisdom et al. 1996), so we do not focus further on them.

The situation is completely different for chaotic orbits. Rein et al. (2019) studied the effect of Hamiltonian smoothness during a short-term chaotic simulation which integrates over discontinuities twice or four times, except in the modified-Heaviside case. The errors were studied using approximations to commutators which may or may not converge. Rein et al. (2019) argued that over this short-term simulation, Hamiltonian smoothness made no significant impact. However, the advantage of symplectic integrators is in their long-term behavior.

In this work, we study whether the symmetry of C^∞ Hamiltonian smoothness should be enforced for chaotic orbits for long time-scales (many orbital periods). We consider hybrid integrators, as in Hernandez (2019), because their smoothness is easy to tune. We construct a hybrid N -body integrator combining ideas from Chambers (1999), Rein et al. (2019), and Wisdom (2017). According to the modified differential equations (MDEs) (Hernandez & Bertschinger 2018; Hairer et al. 2006), we predict Hamiltonian smoothness should have a significant impact on the error of integrators. To test these ideas, we consider a restricted three-body problem in which the test particle executes a chaotic orbit in which it can visit both masses. We observe integrator performance improvement by increasing the smoothness from $n=0$ to $n=4$. The error of the integrator apparently saturates for higher n . The MDEs suggest that the effects of nonsmoothness, for this particular hybrid integrator, should disappear as the timestep approaches 0. We verify this numerically by rerunning our test with a step 10 times smaller. This work provides evidence that the smoothness of the N -body problem is a symmetry which should be followed as closely as possible by N -body integrators. This is not the case for the other methods described above such as block time-stepping.

In Section 2 we show how we construct the hybrid N -body integrators. We carry out error analysis of a similar hybrid integrator using MDEs in Section 3 and give an example of how a non-smooth function leads to secular error. Numerical experiments demonstrating the significance of Hamiltonian smoothness are carried out in Section 4. Section 5 concludes and discusses the impact of this work on N -body integrators.

2 ALGORITHM DESCRIPTION

To construct a hybrid N -body integrator, we combine ideas from Chambers (1999) and Wisdom (2017). A coordinate system must be chosen. Jacobi coordinates (Hernandez & Dehnen 2017) are problematic because we cannot use the natural Kepler solutions for bodies not undergoing close encounters. This problem was pointed out by Chambers (1999). Jacobi coordinates are appropriate if massive bodies cannot have close encounters, but massless test particles can have close encounters with the massive bodies. This was the situation studied by Wisdom (2017). We thus use Democratic Heliocentric coordinates (Hernandez & Dehnen 2017), which accommodate both massive and massless possibly having close encounters. The Hamiltonian in these coordinates is split into two parts, A and B , given by (Chambers 1999):

$$A = T_1 + V_\odot + V_{p1} \quad \text{and} \quad (1a)$$

$$B = T_0 + V_{p2}. \quad (1b)$$

We defined,

$$\begin{aligned} T_1 &= \sum_{i \neq 0} \frac{P_i^2}{2m_i}, & V_\odot &= - \sum_{i \neq 0} \frac{Gm_0 m_i}{Q_i}, \\ V_{p1} &= - \sum_{0 < i < j} \frac{Gm_i m_j}{Q_{ij}} (1 - K(Q_{ij})), \\ T_0 &= \frac{1}{2m_0} \left(\sum_{i \neq 0} P_i \right)^2, & \text{and} & \quad V_{p2} = - \sum_{0 < i < j} \frac{Gm_i m_j}{Q_{ij}} K(Q_{ij}). \end{aligned} \quad (2)$$

K is a function such that $0 \leq K \leq 1$. A is Liouville integrable if all K equal 1. Then, a Kepler advancer such as that of Wisdom & Hernandez (2015) can be used to solve it. Otherwise, A , is not described by periodic orbits, and numerical approximation methods, such as those relying on computing Taylor series solutions to the ordinary differential equations (ODEs) to high powers in an expansion parameter must be used. B is always integrable and simple to solve. A and B both conserve linear and angular momentum, which we verified numerically.

We construct an integrator using

$$e^{h\hat{H}} = e^{\frac{h}{2}\hat{B}} e^{h\hat{A}} e^{\frac{h}{2}\hat{B}} \quad \text{or} \quad (3a)$$

$$e^{h\hat{H}} = e^{\frac{h}{2}\hat{A}} e^{h\hat{B}} e^{\frac{h}{2}\hat{A}}, \quad (3b)$$

where h is a timestep. Chambers (1999) and Rein et al. (2019) used the first version, BAB . We call the second version ABA . The $n=1$ planet problem (the Kepler problem) is not solved exactly by these integrators. To see this, let the maximum i in Eqs. (1) and (2) be 1. This problem has a solution, involving modifying the terms placed in A and B . (Hernandez & Dehnen 2017, Section 4.2) showed how to do this when all $K=0$, but the generalization to allow other K is immediate. We tested this alternative splitting, but it did not perform better in the tests in this paper because solving the $n=1$ problem is not the only consideration for a good integrator (Hernandez & Dehnen 2017, Figure 6, and error analysis). \hat{H} is given by the BCH formula (Hairer et al. 2006) as,

$$\tilde{H}^{BAB} = A + B + \frac{h^2}{12} \{\{B, A\}, A\} - \frac{h^2}{24} \{\{A, B\}, B\} + \mathcal{O}(h^4), \quad (4)$$

$$\tilde{H}^{ABA} = A + B - \frac{h^2}{24} \{\{B, A\}, A\} + \frac{h^2}{12} \{\{A, B\}, B\} + \mathcal{O}(h^4). \quad (5)$$

$\{\}$ are Poisson brackets. If all K are 1, the Poisson bracket terms are given by Hernandez & Dehnen (2017):

$$\{\{A, B\}, B\} = \{\{V_\odot, T_0\}, T_0\} + \{\{T_1, V_{p1}\}, V_{p1}\} \propto \epsilon^3 \quad \text{and} \quad (6a)$$

$$\begin{aligned} \{\{B, A\}, A\} &= \{\{T_0, V_\odot\}, V_\odot\} + \{\{V_{p1}, T_1\}, T_1\} \\ &\quad - \{\{T_1, V_{p1}\}, V_\odot\} - \{\{V_\odot, T_0\}, T_1\} \propto \epsilon^2. \end{aligned} \quad (6b)$$

If all $K=0$, the Poisson brackets are,

$$\{\{A, B\}, B\} = \{\{V_\odot, T_0\}, T_0\} \propto \epsilon^3 \quad \text{and} \quad (7a)$$

$$\{\{B, A\}, A\} = \{\{T_0, V_\odot\}, V_\odot\} - \{\{V_\odot, T_0\}, T_1\} \propto \epsilon^2. \quad (7b)$$

$\epsilon = m/m_0$, where the largest planetary mass m can be used to give an upper bound on the error scaling. ϵ is assumed to be small. Thus, the ABA form has a lower error in the two limits. We performed numerical experiments of this prediction by integrating a system composed of the Sun, Jupiter, and Saturn. We tested three cases: K was always 0, K was always 1, and K allowed to enter $0 < K < 1$, using a C^2 (see Section 4) K . We used a variety of stepsizes and integration times. In all cases, the absolute magnitude of the energy error was about twice smaller in the ABA case, as compared to BAB . ABA is approximately just as expensive as BAB because

evolving the final A from a step can be combined with evolving the first A of the next step. In this paper, we use the *BAB* integrator form in our tests, but we note that the efficiency can be improved by using *ABA*. The goal of this paper is not to optimize efficiency. The equations of motion for Hamiltonian A are (Rein et al. 2019),

$$\dot{\mathbf{Q}}_i = \mathbf{V}_i \quad (8)$$

$$\dot{\mathbf{V}}_i = -\frac{Gm_0}{Q_i^3}\mathbf{Q}_i - G \sum_{j \neq i, j > 0} \frac{m_j}{Q_{ij}^3} \mathbf{Q}_{ij} (1 - K(Q_{ij}) + Q_{ij}K'(Q_{ij})), \quad (9)$$

where $\mathbf{V}_i = \mathbf{P}_i/m_i$ is the barycentric velocity. Using velocities instead of momenta is one way to ensure we can describe test particles. We used (Rein et al. 2019),

$$\frac{\partial K(Q_{ij})}{\partial Q_{ij}} = \frac{Q_{ij}}{Q_{ij}} \frac{\partial K(r)}{\partial r} \Big|_{r=Q_{ij}} = \frac{Q_{ij}}{Q_{ij}} K'(Q_{ij}). \quad (10)$$

The equations for Hamiltonian B are,

$$\dot{\mathbf{Q}}_i = \frac{1}{m_0} \sum_{i \neq 0} \mathbf{P}_i \quad (11)$$

$$\dot{\mathbf{V}}_i = -G \sum_{j \neq i, j > 0} \frac{m_j}{Q_{ij}^3} \mathbf{Q}_{ij} (K(Q_{ij}) - Q_{ij}K'(Q_{ij})) \quad (12)$$

Since $\dot{\mathbf{Q}}_i$ is 0, \mathbf{Q}_i is a constant. $\dot{\mathbf{V}}_i$ is constant because $\dot{\mathbf{Q}}_{ij}$ is 0.

3 MODIFIED DIFFERENTIAL EQUATIONS

Although we have written the equations of motion for A and B , the integrators of (3) can be described by sets of ODEs called modified differential equations (MDEs) (Hernandez & Bertschinger 2018). We derive these for the first-order integrator,

$$e^{h\hat{H}} = e^{h\hat{A}} \circ e^{h\hat{B}}. \quad (13)$$

The Section 3.1 example also uses a first order integrator. Here,

$$\hat{H} = T_1 + T_0 + V_\odot + V_{p1} + V_{p2} + \frac{h}{2} (\{V_{p2}, T_1\} + \{T_0, V_\odot\}) + \mathcal{O}(h^2). \quad (14)$$

The set of ODEs comes from \hat{H} . For $i > 0$,

$$\dot{\mathbf{Q}}_i = \frac{\partial \hat{H}}{\partial \mathbf{P}_i} = \mathbf{a}_{0i} + \mathbf{a}_{1i}h + \mathcal{O}(h^2), \quad \text{and} \quad (15a)$$

$$\dot{\mathbf{V}}_i = -\frac{1}{m_i} \frac{\partial \hat{H}}{\partial \mathbf{Q}_i} = \mathbf{b}_{0i} + \mathbf{b}_{1i}h + \mathcal{O}(h^2), \quad (15b)$$

We defined,

$$\mathbf{a}_{0i} = \frac{\mathbf{P}_i}{m_i} + \frac{\mathbf{P}_\odot}{m_0}, \quad (16a)$$

$$\mathbf{a}_{1i} = \frac{1}{2} \left(\sum_{j \neq i, j > 0} \frac{Gm_j}{Q_{ij}^3} \mathbf{Q}_{ij} (K(Q_{ij}) - Q_{ij}K'(Q_{ij})) + \sum_{j > 0} \frac{Gm_j}{Q_j^3} \mathbf{Q}_j \right), \quad (16b)$$

$$\mathbf{b}_{0i} = -\frac{Gm_0}{Q_i^3} \mathbf{Q}_i - \sum_{j \neq i, j > 0} \frac{Gm_j}{Q_{ij}^3} \mathbf{Q}_{ij}, \quad \text{and} \quad (16c)$$

$$\begin{aligned} \mathbf{b}_{1i} = & -\frac{1}{2} \left(\sum_{j \neq i, j > 0} \frac{Gm_j}{Q_{ij}^5} \left[(-3\mathbf{Q}_{ij}(\mathbf{Q}_{ij} \cdot \mathbf{V}_{ij}))(K(Q_{ij}) - Q_{ij}K'(Q_{ij})) \right. \right. \\ & \left. \left. + 1/3 Q_{ij}^2 K''(Q_{ij}) - \mathbf{V}_{ij} Q_{ij}^2 (K(Q_{ij}) - Q_{ij}K'(Q_{ij})) \right] \right) \\ & + \frac{G}{Q_i^5} \left[-3\mathbf{Q}_i(\mathbf{Q}_i \cdot \mathbf{P}_\odot) + \mathbf{P}_\odot Q_i^2 \right], \end{aligned} \quad (16d)$$

where $\mathbf{P}_\odot = \sum_{i > 0} \mathbf{P}_i$ (Hernandez & Dehnen 2017). Eqs. (15) are not Taylor series in h : h is a constant parameter. The MDEs do not need to converge in h , they correctly describe the dynamics. Eqs. (16) are generally nonzero for massive and massless particles. \mathbf{a}_{0i} is the heliocentric velocity and \mathbf{b}_{0i} is the Newtonian force: in the limit $h \rightarrow 0$, these are the only surviving terms and the MDEs exactly solve the gravitational N -body equations. We can see that the integrator (13) suffers from the same problem as integrators (3), and any integrator split into the A and B from (1): the $n = 1$ problem is not solved exactly, even when $K(Q_{ij})$ and its derivatives are 0. We see this because terms \mathbf{a}_{1i} and \mathbf{b}_{1i} are nonzero, although $\mathbf{a}_{1i} = 0$ for test particles. The coefficients as the power of h increases depend on higher derivatives of K . Up to first order in h , two derivatives of K are needed. As we integrate these MDEs over discontinuities in those derivatives, unresolved timescales can occur (Hernandez 2019), leading to large errors. As h is increased, these discontinuities will become more important. The MDEs corresponding to integrator *BAB*, Eq. (3a), also the one considered in Chambers (1999) and Rein et al. (2019), do not have form (15); the leading error term is $\mathcal{O}(h^2)$. However, Eqs. (15) and (16) let us see how discontinuities would enter any MDEs in which derivatives of K at some order are undefined.

3.1 Example error analysis

Here we show and explain an example of non-smoothness giving rise to secular errors. This subsection can be omitted without loss of continuity. Consider the simple harmonic oscillator (SHO), with Hamiltonian,

$$H = \frac{p^2 + q^2}{2}. \quad (17)$$

We are concerned in this work with chaotic orbits, but for this example, we use a periodic orbit. We construct a hybrid integrator to solve this problem. This integrator was considered in (Hernandez 2019, Section 4.1). The Hamiltonian is split into,

$$H_1 = \frac{q^2 K(q) + p^2}{2} \quad \text{and} \quad H_2 = \frac{q^2(1 - K(q))}{2}. \quad (18)$$

The integrator is,

$$e^{h\hat{H}} = e^{h\hat{H}_2} \circ e^{h\hat{H}_1}. \quad (19)$$

H_1 is solved using Bulirsch–Stoer (as in Hernandez (2019)). Let $x =$

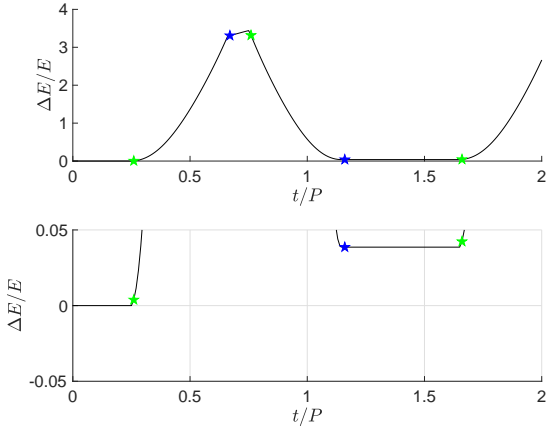


Figure 1. Energy error as a function of time for an integration with the SHO integrator, (19). Initially, $q = 1$ and $p = 0$. A time step $h = P/100$ is used, where $P = 2\pi$ is the exact SHO period. Four steps integrate over a discontinuity in the first period—they are indicated with stars. A green star locates the end of a time step where an integration out of the region $0 < K < 1$ was performed. A blue star indicates an integration into the region $0 < K < 1$. The bottom panel is a zoomed in region of the top panel. In it, the floor of the energy error shifts $\approx +0.035$. This is explained with error analysis in Section 3.1.

$(q+2)/2$. If $x < 0$, $K(q) = 0$. If $x > 0$, $K(q) = 1$. Otherwise, $K(q) = x$. This K is a C^0 function, so integrator (19) is not symplectic, according to Hernandez (2019). As in Hernandez (2019), initially, $q = 1$ and $p = 0$. $h = P/100$, where the exact period is $P = 2\pi$. The runtime is $t = 2P$. The energy error as a function of time is plotted in Fig. 1.

In the first period, four steps, shown with stars, integrate over a discontinuity. By ‘discontinuity,’ we refer to discontinuities in dK/dr . Stars locate the end of those steps. A green star means the region $0 < K < 1$ was left, while a blue star means $0 < K < 1$ was entered. The bottom subpanel zooms in on a portion of the top subpanel, and shows the energy error floor shifting. We now explain the magnitude and sign of this shift. A succession of such shifts lead to long-term error deterioration.

First, we calculate \tilde{H} , given by the BCH formula. If the series converges, we can ignore high powers in h and assume \tilde{H} is conserved. We have,

$$\tilde{H} = H + \frac{h}{2} \{H_1, H_2\} + O(h^2), \quad (20)$$

The Poisson brackets are calculated as,

$$\{H_1, H_2\} = p \left(\frac{q^2}{2} \frac{dK}{dq} - q(1-K) \right). \quad (21)$$

Note that \tilde{H} describes exact, continuous dynamics, explained by MDEs, although the integrator samples discrete points along the solution path. We calculate the error across a discontinuity. Using (20) and (21), and ignoring higher h powers,

$$\delta = \frac{\Delta H}{H_0} = \frac{-\frac{h}{2} \left(\{H_1, H_2\} \Big|_+ - \{H_1, H_2\} \Big|_- \right)}{H_0} = sapq^2. \quad (22)$$

H_0 is the initial energy ($1/2$). $\Big|_+$ indicates the limit from the right (forward time) of the discontinuous point while $\Big|_-$ is the limit from

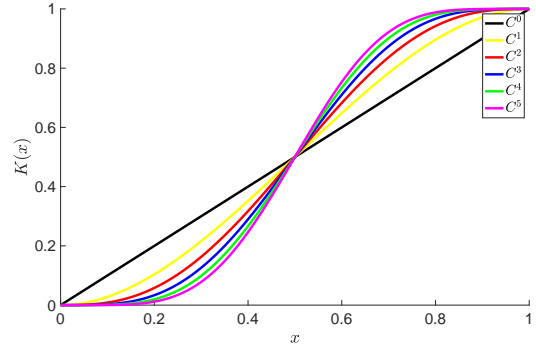


Figure 2. We plot the transition functions considered in this work. The functions are labelled C^n , where n is the number of derivatives that are continuous. The functions are all smooth, except at $x = 0$ and $x = 1$. The linear C^0 function is continuous, but not differentiable.

the left. $a = h/(8H_0)$. s is $+1$ if $0 < K < 1$ was entered while it is -1 if $0 < K < 1$ was left. We calculate the first four δ values of Fig. 1 approximately, because only data at discrete values is available from the integrator. We use the coordinates after integrating over the discontinuity. Labelling each δ , $\delta_1 = -6.2 \times 10^{-5}$, $\delta_2 = 0.027$, $\delta_3 = 0.039$, and $\delta_4 = -5.8 \times 10^{-5}$. The maximum δ and maximum pq^2 are, respectively, 0.039 and ≈ 2.5 . The jump in the bottom sub-panel of Fig. 1 is $+0.035$, so this error analysis provides an approximation for this jump. Reducing the step by 10 to $h = P/1000$, there are again four discontinuities over the first period. The maximum magnitude of pq^2 is similar, ≈ 2.3 , and a is 10 times smaller. The error floor jumps in this case by $+0.004$, and the error analysis result again matches approximately the data.

4 NUMERICAL EXPERIMENTS

We return attention to the N -body problem. We have yet to specify the functional form of K . To discuss K , first consider a function $x = (r - h_1R)/(h_2R)$, the function considered by Wisdom (2017). r is the separation between two non-solar bodies, and R is a constant. If $x < 0$, $K = 0$. If $x > 1$, $K = 1$. Otherwise, we consider the following progressively smoother functions,

- (i) C^0 : $K = x$
- (ii) C^1 : $K = -2x^3 + 3x^2$
- (iii) C^2 : $K = 6x^5 - 15x^4 + 10x^3$
- (iv) C^3 : $K = -20x^7 + 70x^6 - 84x^5 + 35x^4$
- (v) C^4 : $K = 70x^9 - 315x^8 + 540x^7 - 420x^6 + 126x^5$
- (vi) C^5 : $K = -252x^{11} + 1386x^{10} - 3080x^9 + 3465x^8 - 1980x^7 + 462x^6$

The functions increase monotonically and have odd-symmetry about $x = 1/2$. They are displayed in Fig. 2. Following Wisdom (2017), if, for a given pair, $x > h_3R$ at the start of A , we use Kepler solvers to solve the Hamiltonian terms with their indices i and j . $h_3R > 1$ by construction. Otherwise, Bulirsch–Stoer is used for that pair in A , to account situations in which K becomes less than 1 during the evolution of the A Hamiltonian.

We consider a simple chaotic system with two degrees of freedom, the restricted three-body problem. It has one constant of motion. In an inertial frame it is,

$$C_J = \frac{1}{2}v^2 + \Phi(x) - \omega \cdot (x \times v), \quad (23)$$

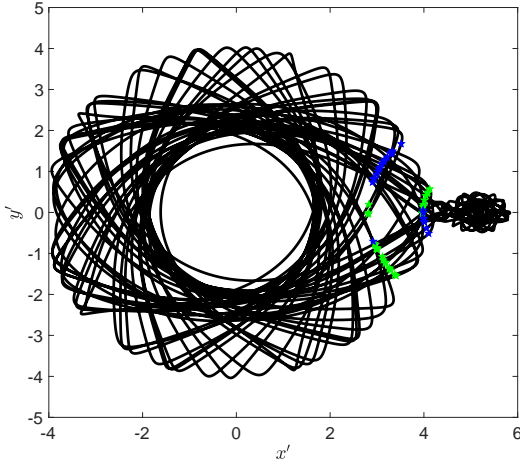


Figure 3. The trajectory in the rotating frame of the test particle in the restricted three-body problem described in Section 4. The initial conditions are (25). The *BAB* integrator is used with $h = 8$ days and the C^2 transition function. The total runtime is 500 yrs. Green and blue stars indicate a step with an integration over a discontinuity. Green stars mean the test particle left the region $0 < K < 1$, while blue stars mean the particle entered the $0 < K < 1$ region. Note we have not used red to draw the C^2 curve as in Fig’s. 2, 4, 5, and 6.

where ω is the binary angular velocity, $\omega = \sqrt{G(m_1 + m_2)/a^3} \hat{z}$, and

$$\Phi(\mathbf{x}) = -\frac{Gm_1}{|\mathbf{x} - \mathbf{x}_1|} - \frac{Gm_2}{|\mathbf{x} - \mathbf{x}_2|}. \quad (24)$$

a is the semi-major axis, m_1 and m_2 are the stellar and planetary mass, respectively, and \mathbf{x}_1 and \mathbf{x}_2 are their positions. \mathbf{x} and \mathbf{v} are the position and velocity of the test particle. In units of au, day, and solar masses, the test particle has heliocentric position and velocity

$$\begin{aligned} \mathbf{x} &= (4.42, 0) \\ \mathbf{v} &= (0, 0.0072). \end{aligned} \quad (25)$$

$m_1 = 1$ and m_2 is defined through $\mu = m_2/(m_1 + m_2) = 0.01$. $a = 5.2$. Initially, all bodies are aligned with the x -axis, with the star on the left. The center of mass is at 0. This problem was considered by Wisdom (2017), so a comparison is possible in integrator performance. We let R be the m_2 Hill radius, $R = a(m_2/(3m_1))^{1/3}$, $h_1 = h_2 = 1.5$, and $h_3 = 4.0$, as in Wisdom (2017). For all tests in this paper, we checked that when Kepler solvers were used to solve A , a close encounter condition, $K < 1$, was not detected after evolving the A Hamiltonian. This justifies the choice of h_3 .

Using the C^2 K , $h = 8$ days, and running for a total time $t = 500$ yrs, we show the trajectory in the rotating frame in Fig. 3. We have also indicated with green stars if a transition out of the region $0 < K < 1$ happened during the timestep yielding the coordinates. This means an integration over a discontinuity was performed. We also show with blue stars when a transition into $0 < K < 1$ happened. 54 steps integrated over a discontinuity, out of a total of 22,830 steps. Transitions should occur at separations of $r = 3.0R$ and $r = 1.5R$, respectively, which we verified numerically.

Next, we measure the Jacobi constant error for long-term integrations over 10,000 yrs using various smoothing functions. We expect that smoother functions will have better error. We use $h = 8$ days, but to reduce variations in the error, we plot the median error every 1000 steps, so that a total of 456 points are plotted. We also

plot data from Wisdom (2017), Figure 9. For these data, median absolute errors every 20 steps are plotted, so that there are also a total of 456 points in the range $t = 0$ to $t = 10,000$ yrs. We indicate by integers n the smoothness: C^n is the smoothness. The result is shown in Fig. 4.

Integrations with smoother transition functions have smaller error, although there is no significant improvement from $n = 4$ to $n = 5$. We can improve on the Wisdom (2017) data simply by increasing smoothness at virtually no additional cost. Running to 500 yrs, the C^5 experiment took about 1% longer in wall-clock time than the C^2 test. The C^5 test was faster than the C^0 test, but note different runs may have a different number of evaluations of the polynomial function. We used the MATLAB software for this timing test. But our goal is not to improve on the Wisdom (2017) result—if our focus were on accuracy, we could reduce the error on all our curves by using instead the *ABA* forms. Our goal is to demonstrate the importance of the transition function.

Because the error as a function of time strongly depends on the initial conditions, we want to see if our results hold for a variety of orbits. Thus, we perturb the initial conditions (25), but not so much that the initial conditions’ Jacobi constant no longer satisfies the condition for a chaotic exchange orbit (Dehnen & Hernandez 2017, Section 3.3). For the test of Fig. 3, the variation in either test particle position coordinate is ≈ 10 , while the variation in either velocity is ≈ 0.03 . Thus, we set a position and velocity scale as $x_s = 10$ and $v_s = 0.01$, respectively. Then 8 initial conditions are generated by perturbing one of the positions or velocities at a time from the initial conditions above. The positions are perturbed by $\pm x_s \delta$ and velocities by $\pm v_s \delta$, where $\delta = 10^{-3}$. For the long timescales we study in our tests, we can perturb initial conditions even by small amounts like 10^{-15} . Assuming a Lyapunov time of 4 yrs, if we perturb the initial conditions by 10^{-15} , the trajectories will differ by unity after ≈ 136 yrs. However, in one such test, significant differences between orbits were not apparent until after 400 yrs. We repeat the test from Fig 4, but with 8 initial conditions with each transition function. We plot their errors by again taking median values and using thin lines. A thick line represents an average in log space, or the geometric mean, of the eight curves. The result is shown in Fig. 5. This plot confirms the improvement in error from increasing smoothness. As in Fig. 4, there is improvement in error until $n = 4$. It is unclear whether this is an improvement from $n = 4$ to $n = 5$.

We verified the orbits from nearby initial conditions diverge quickly. For a certain integrator and the unperturbed initial conditions (25), Dehnen & Hernandez (2017) reported a Lyapunov time of 4 yrs. For the $n = 2$ case, we compared the orbit in which the x coordinate is perturbed by $-x_s \delta$ and the orbit for which y is perturbed by $+x_s \delta$. We calculated the Euclidean norm of the distance between the two orbits, which reached unity before 5 yrs. The Euclidean norm in velocity space reached its saturation of approximately 10^{-2} at a similar time.

Based on the MDEs from (15), we expect that as h is decreased, the smoothness of the transition will matter less, as its impact on the error becomes smaller. To show this, we rerun the initial conditions (25) and their 8 perturbed orbits using a step 10 times smaller, $h = 0.8$ days. Median values are taken every 10,000 steps for plotting, so that the same number of points are plotted as in Fig. 5. We compare the Jacobi constant errors in Fig. 6 between the two timestep runs, up to $t = 1,000$ yrs. The top panel uses $h = 0.8$ days. There is no clear difference once $n > 1$ in this case, while for $h = 8$ days case, differences are hard to see for $n > 2$. Also note all thick curves have smaller error for the $h = 0.8$ days case.

Finally, we want to demonstrate that large errors in the Ja-

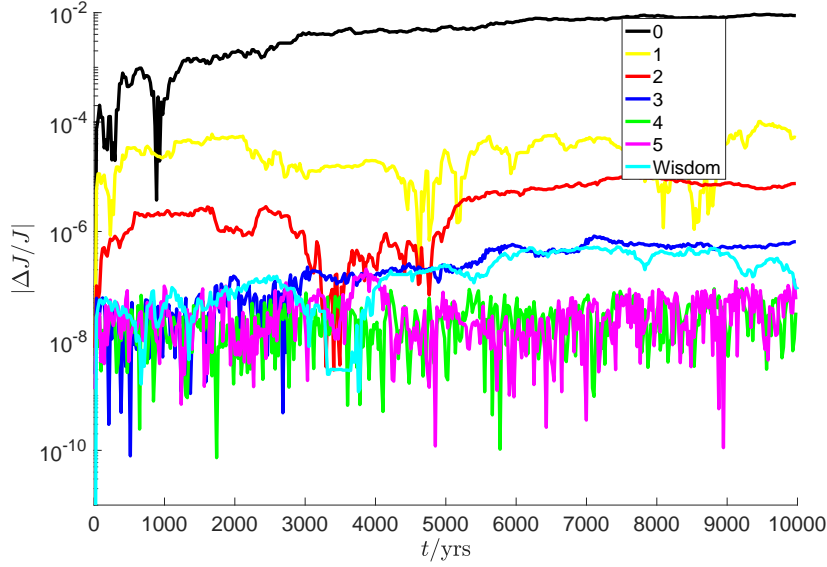


Figure 4. The absolute value of the error of the Jacobi constant, eq. (23), for the restricted three-body problem considered by Wisdom (2017). The *BAB* integrator with step $h = 8$ days is used with different transition functions. The legend denotes n , where C^n is the smoothness. We have also plotted data from Wisdom (2017), Figure 9, kindly provided by Jack Wisdom. Increasing the smoothness improves the error by nearly five orders of magnitude and even improves on the Wisdom (2017) data.

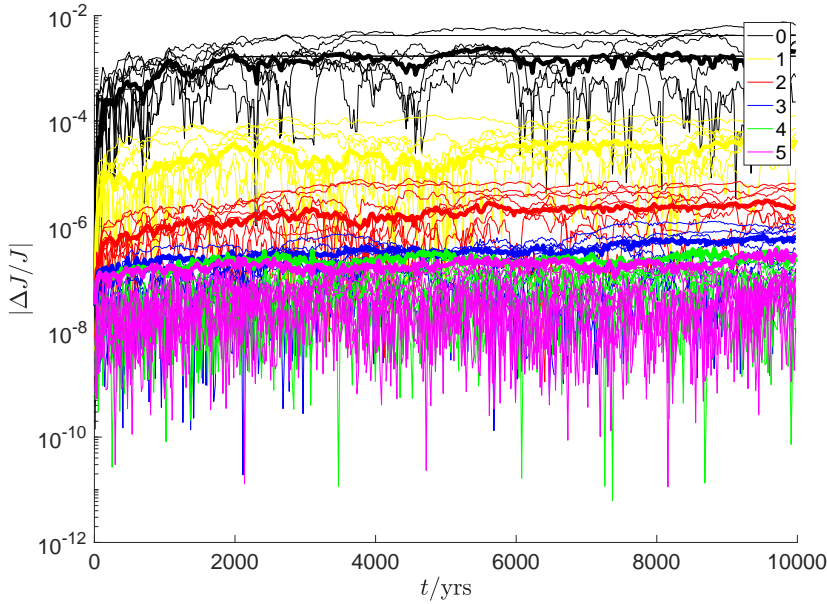


Figure 5. The same test is run as in Fig. 4, but for each transition function, 8 initial conditions are run. Each is indicated with a thin line. Thick lines indicate the geometric mean of the thin lines. The improvement in error with smoothness observed in Fig. 4 is a robust result that does not depend on a particular choice of initial conditions.

cobi constant are associated with integrations over discontinuities. In Fig. 7 we plot the error in the Jacobi constant for the C^2 function over the first 50 yrs, using $h = 8$ days. We also plot when an integration over a discontinuity occurred. We find the first discontinuity is associated with a secular increase in the Jacobi constant error. Further discontinuities are associated with other error spikes.

5 CONCLUSION

Symplectic integration has been popular and successful at describing astrophysical N -body and other dynamics. Symplectic integration is part of a broader category of integration called geometric integration (Hairer et al. 2006) in which solutions to ordinary differential equations (ODEs) are calculated through approximations which respect ‘geometric’ features of the ODEs. This is useful for

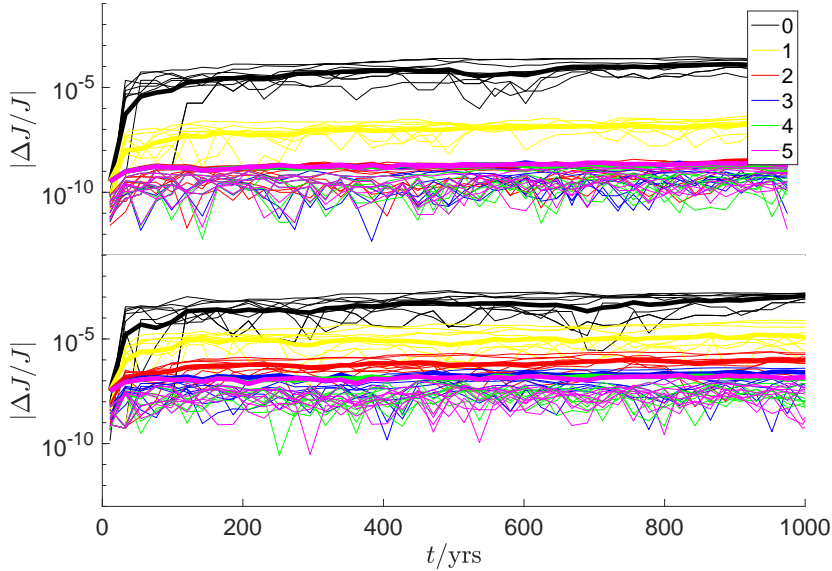


Figure 6. We compare how the impact of smoothness on error depends on the time step. The bottom panel uses data from Fig. 5. The top panel is the same integration with step 10 times smaller, $h = 0.8$ days. As predicted, smoothness makes less of an impact in the top panel. Note the runtimes are only 1,000 yrs.

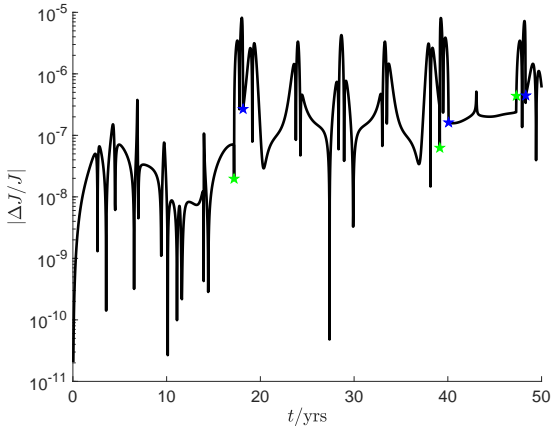


Figure 7. We show that integrations over discontinuities lead to error increases. This plot takes the first 50 years from the C^2 function in Fig. 4. Stars indicate a step where an integration over a discontinuity occurred. The meaning of the stars is the same as in Fig. 3. Note we have not used red to draw the C^2 curve as in Fig's. 2, 4, 5, and 6.

any long-term dynamical studies. Symplectic integration is supposed to conserve the Poincaré invariants associated with Hamiltonian dynamics, leading to bounded errors over long time intervals. Popular symplectic integrators (Wisdom & Holman 1991; Springel 2005) also aim to preserve the other geometric features of the ODEs: the time-symmetry, and the angular and linear momentum conservation.

Another geometric feature which is perhaps overlooked is the smoothness of an integrator. The N -body Hamiltonian is infinitely smooth, or C^∞ for physical separations greater than 0. Symplec-

tic integrators are described by modified differential equations, which are also derived from a Hamiltonian with some smoothness. A number of popular symplectic methods, and perhaps the most versatile and useful ones (Chambers 1999; Duncan et al. 1998; Springel 2005) are only C^n smooth, where n is a small integer, or worse, one might argue a smoothness concept is not applicable to them. Any method with adaptive block stepping also has reduced smoothness. This work has explored the role of smoothness in the accuracy of N -body integrations. To explore this question, we have considered hybrid (Chambers 1999; Rein et al. 2019; Wisdom 2017; Hernandez 2019) integrators, whose smoothness is easily tuned through a switching function. Hybrid integrators are C^∞ in most of phase space, except for a few points in phase space which are rarely or never hit, in which there is smaller smoothness (except if an expensive C^∞ transition function is used). However, Hernandez (2019) has shown that the performance of hybrid integrators degrades for regular orbits even when those points are never encountered in practice, and explained why.

This work has focused on the broad class of chaotic orbits, and how their errors might be affected by smoothness of the method. We have provided evidence that Hamiltonian smoothness has significant impacts on N -body performance. In a test first considered by Wisdom (2017) of a restricted three-body problem, the integrator performance significantly improved as n was increased from 0 to 4 by about 5 orders of magnitude in the Jacobi constant error. We argued that this result can be explained through the MDEs. We also verified the expectation that smoothness should become less important as the timestep goes to 0. Our results indicate that just as using symplectic integrators has become a pillar of dynamical astronomy, using integrators that are as smooth as possible is a consideration which is arguably just as important. Increasing smoothness may not be easy to do in the case of block time-stepping methods, but for

other methods, like hybrid integrators, increasing smoothness may be negligibly more computationally expensive, as we explored.

We remark on the relationship between smoothness and symplecticity: [Hernandez \(2019\)](#) has argued that a symplectic integrator should have at least $C^{1,1}$ smoothness (C^1 and Lipschitz continuous in the ODEs), because these guarantee the existence of periodic orbits. This was verified numerically, and was predicted by [Arnaud & Xue \(2016\)](#), with some caveats described in [Hernandez \(2019\)](#). According to this criteria, we have explored both symplectic and non-symplectic integrators in this work, depending on the smoothness of the transition function.

Finally, we note that we have not investigated in detail the role smoothness plays in nonsymplectic integrators, but it is reasonable to assume smoothness can improve any integrator described by MDEs, symplectic or not.

6 ACKNOWLEDGEMENTS

I thank Jun Makino, Scott Tremaine, and Matt Payne for comments.

REFERENCES

- Arnaud M.-C., Xue J., 2016, A C^1 Arnol'd-Liouville theorem, working paper or preprint, <https://hal-univ-avignon.archives-ouvertes.fr/hal-01422530>
- Boekholt T., Portegies Zwart S., 2015, *Computational Astrophysics and Cosmology*, 2, 2
- Chambers J. E., 1999, *MNRAS*, 304, 793
- Dehnen W., Hernandez D. M., 2017, *MNRAS*, 465, 1201
- Duncan M. J., Levison H. F., Lee M. H., 1998, *AJ*, 116, 2067
- Farr W. M., Bertschinger E., 2007, *ApJ*, 663, 1420
- Hairer E., Lubich C., Wanner G., 2006, *Geometrical Numerical Integration*, 2nd edn. Springer Verlag, Berlin
- Hernandez D. M., 2019, arXiv e-prints, p. [arXiv:1902.03684](https://arxiv.org/abs/1902.03684)
- Hernandez D. M., Bertschinger E., 2018, *MNRAS*, 475, 5570
- Hernandez D. M., Dehnen W., 2017, *MNRAS*, 468, 2614
- Portegies Zwart S., Boekholt T., 2014, *ApJ*, 785, L3
- Rein H., et al., 2019, arXiv e-prints, p. [arXiv:1903.04972](https://arxiv.org/abs/1903.04972)
- Springel V., 2005, *MNRAS*, 364, 1105
- Wisdom J., 2017, *MNRAS*, 464, 2350
- Wisdom J., Hernandez D. M., 2015, *MNRAS*, 453, 3015
- Wisdom J., Holman M., 1991, *AJ*, 102, 1528
- Wisdom J., Holman M., Touma J., 1996, *Fields Institute Communications*, Vol. 10, p. 217, [10, 217](#)
- Yoshida H., 1990, *Physics Letters A*, 150, 262